*FUDMA Journal of Sciences (FJS)*
*ISSN online: 2616-1370*
*ISSN print: 2645 - 2944*
*Vol. 3 No. 3, September, 2019, pp 131 –138*

# COMPARISON OF GEOPHYSICAL PARAMETERS OF GEOELECTRIC SECTION AND SEISMIC REFRACTION IMAGING ALONG THE SAME PROFILE ACROSS A BOREHOLE LOCATION AT AGBAN-KAGORO, KADUNA STATE NIGERIA

**AFUWAI GWAZAH CYRIL**

Department of Physics, Kaduna State University, Kaduna-Nigeria

Corresponding authors email: cyril.afuwai@kasu.edu.ng, +2348029004763

**ABSTRACT**

Geophysical survey was carried out across a functional borehole with the aim to compare the geophysical parameters of Geoelectric section and seismic refraction tomography taken along the same profile. In the Geoelectric section ten (10) VES Points were taken at 5m interval along the W-E direction across the borehole, five (5) subsurface layers were detected; the topsoil comprising wet sandy clay, the weathered basement which constitutes of water and sand with little traces of sandy clay at VESagb8, the partially weathered basement with resistivity range of 133-178Ωm composed of fine grain sand, the fractured basement comprises of coarse grain sand with resistivity range of 237-316Ωm, the fifth layer is the fresh basement rock. The Seismic refraction tomography is predominantly characterized by four (4) layers having relatively low p-wave velocities (327m/s) at its uppermost layers and relatively high velocities of over 2420m/s at depths. The range of the velocity measured (327 - 2500 m/s) encompasses the p-wave velocities of sand (320 - 800 m/s), sandy clay (850 - 1250m/s) and clay (900 – 25000 m/s) which occur at shallow depths (24m) while at depths, occur coarse grain sand (weathered basement) of p-wave velocities (1500-30000m/s) and porphyritic granite (fresh basement) of range 2000–45000 m/s. Aquiferous zones (1200 m/s – 1500 m/s) occur between the depths of 12m and 25m. Generally, the survey shows a high correlation of the earth materials along the profile for both the resistivity and seismic refraction surveys.

**Keywords:** Borehole, Geoelectric, Seismic refraction, Aquiferous zones

## INTRODUCTION

Geophysical investigation of subsurface structures uses the principles of physics to study the Earth's subsurface features and nature of the underlying geology. For some times now the use of Seismic Refraction Tomography (SRT) and Electrical Resistivity Tomography (ERT) for subsurface investigations has greatly improved the quality of acquired data for two- and three-dimensional surveys. SRT employs more shot points and receivers than the conventional seismic refraction for its imaging technique. ERT uses automated multi-electrode array systems to improve the resolution of large data collection (Adedibu and Abimbola, 2019). SRT and ERT techniques use powerful inversion algorithms to achieve high resolution subsurface inversion models for resolving subsurface characteristics and geological conditions over a complex and larger area that may be difficult with the use of their conventional methods. These state-of-the-art techniques have extensively been used for groundwater, environmental, engineering and mining investigations among others. This study aims to compare data inversion techniques for the seismic refraction tomography and the Geoelectric section in use for subsurface investigations.

### Theory of Electrical Resistivity Method

In the DC resistivity surveying, an electric current is passed into the ground through two outer electrodes (current electrodes), and the resultant potential difference is measured across two inner electrodes (potential electrodes) that are arranged in a straight line, symmetrically about a centre point. The ratio of the potential difference to the current is displayed by the Terrameter as resistance. A geometric factor $\boldsymbol{K}$ in metres is calculated as a function of the electrode spacing. The electrode spacing is progressively increased, keeping the centre point of the electrode array fixed. A and B are current electrodes through which current is supplied into the ground, **M** and **N** are two potential electrodes to measure the potential differences between the two electrodes and P is the VES station to be sounded. The potential difference between the two potential electrodes is measured. The apparent resistivity is given by

$$\boldsymbol{\rho_a = k\left(\frac{\Delta V}{I}\right)} \qquad (1)$$

With K a geometric factor which only depends on electrode spacing and is given by

$$\boldsymbol{K = \pi\left(\frac{L^2}{2b} - \frac{b}{2}\right)} \qquad (2)$$

Electrical resistivity method is defined by their frequency of operation, the origin of the source signals and the manner by which the sources and receivers are coupled to the ground. The method is generally governed by Maxwell's equations of electromagnetism. In the direct-current (DC) frequency, the diffusion term is zero and the field is thus governed entirely by Poisson equation. Electrical methods of geophysical investigations are based on the resistivity (or its inverse, conductivity) contrasts of subsurface materials. The electrical resistance, $\boldsymbol{R}$ of a material is related to its physical dimension,

cross-sectional area, $\boldsymbol{A}$ and length, $\boldsymbol{l}$ through the resistivity, $\boldsymbol{\rho}$ or its inverse, conductivity, $\boldsymbol{\sigma}$ by

$$\boldsymbol{\rho = \frac{1}{\sigma} = \frac{RA}{l}} \quad (3)$$

Low-frequency alternating current is employed as source signals in the DC resistivity surveys in determining subsurface resistivity distributions. Thus, the magnetic properties of the materials can be ignored so that Maxwell's equations of electromagnetism reduced to:

$$\boldsymbol{\nabla . \vec{E} = \frac{1}{\varepsilon_\circ} q} \quad (4)$$

$$\boldsymbol{\nabla \times \vec{E} = 0} \quad (5)$$

Where $\vec{E}$ is electric field in *V/m*, *q* is the charge density in $C/m^3$ and $\boldsymbol{\varepsilon_\circ}$ ($8.854 \times 10^{-12}$ *F/m*) is the permittivity of free space. These equations are applicable to continuous flow of direct current; however, they can be used to represent the effects of alternating currents at low frequencies such that the displacement currents and induction effects are negligible. Usually, a complete homogeneous and isotropic earth medium of uniform resistivity is assumed. For a continuous current flowing in an isotropic and homogeneous medium, the current density $\vec{J}$ is related to the electric field, $\vec{E}$ through Ohm's law

$$\boldsymbol{\vec{J} = \sigma \vec{E}} \quad (6)$$

The electric field vector $\vec{E}$ can be represented as the gradient of the electric scalar potential,

$$\boldsymbol{\vec{E} = \nabla \Phi} \quad (7)$$

The apparent resistivity is the ratio of the potential obtained in-situ with a specific array and a specific injected current by the potential which will be obtained with the same array and current for a homogeneous and isotropic medium of 1Ωm resistivity. The apparent resistivity measurements give information about resistivity for a medium whose volume is proportional to the electrode spacing (Grant and West, 1965). Resistivity is affected more by water content and quality than the actual rock material in porous formations. While aquifers that are composed of unconsolidated materials their resistivity decreases with the degree of saturation and salinity of the groundwater (Afuwai and Lawal, 2013).

The apparent resistivity is the ratio of the potential obtained in-situ with a specific array and a specific injected current by the potential which will be obtained with the same array and current for a homogeneous and isotropic medium of 1Ωm resistivity. The apparent resistivity measurements give information about resistivity for a medium whose volume is proportional to the electrode spacing. Resistivity is affected more by water content and quality than the actual rock material in porous formations. Since the measured resistivity is usually a composite of the resistivity of several layers, the apparent resistivity may be smaller or larger than the real resistivities or in rare cases identical with one of the two resistivity values in a homogeneous surface. The apparent resistivity is the same as the real resistivity in a homogeneous subsurface, but normally a combination of contributing strata. The value of the apparent resistivity obtained with small electrode spacing is called the surface resistivity.

**Electrical Properties of Earth Materials Adopted for the Study**

Electric current flows in earth materials at shallow depths through two main methods. They are electronic conduction and electrolytic conduction. In electronic conduction, the current flow is via free electrons, such as in metals. In electrolytic conduction, the current flow is via the movement of ions in groundwater. In environmental and engineering surveys, electrolytic conduction is probably the more common mechanism. Electronic conduction is important when conductive minerals are present, such as metal sulphides and graphite in mineral surveys. The resistivity of common rocks, soil materials and chemicals (Foster et al, 2000) are shown in figure1. Igneous and metamorphic rocks typically have high resistivity values. The resistivity of these rocks is greatly dependent on the degree of fracturing, and the percentage of the fractures filled with ground water. Thus a given rock type can have a large range of resistivity, from about 1000 to 10 million Ωm, depending on whether it is wet or dry. This characteristic is useful in the detection of fracture zones and other weathering features, such as in engineering and groundwater surveys. Sedimentary rocks, which are usually more porous and have higher water content, normally have lower resistivity values compared to igneous and metamorphic rocks. The resistivity values range from 10 to about 10,000 Ωm, with most values below 1000 Ωm. The resistivity values are largely dependent on the porosity of the rocks, and the salinity of the contained water. Unconsolidated sediments generally have even lower resistivity values than sedimentary rocks, with values ranging from about 10 to less than 1000 Ωm. The resistivity value is dependent on the porosity (assuming all the pores are saturated) as well as the clay content. Clayey soil normally has a lower resistivity value than sandy soil. However, note the overlap in the resistivity values of the different classes of rocks and soils. This is because the resistivity of a particular rock or soil sample depends on a number of factors such as the porosity, the degree of water saturation and the concentration of dissolved salts. The resistivity of groundwater varies from 10 to 100 Ωm. depending on the concentration of dissolved salts. Note the low resistivity (about 0.2 Ωm) of seawater due to the relatively high salt content. This makes the resistivity method an ideal technique for mapping the saline and fresh water interface in coastal areas. One simple equation that gives the relationship between the resistivity of a porous rock and the fluid saturation factor is Archie's Law. It is applicable for certain types of rocks and sediments, particularly those that have low clay content. The electrical conduction is assumed to be through the fluids filling the pores of the rock. Archie's Law is given by

$$\boldsymbol{\rho = a\rho_w \varphi^{-m}} \quad (8)$$

where ρ is the rock resistivity, $\rho_w$ is fluid resistivity, φ is the porosity (fraction of the rock filled with the fluid) while *a* and *m* are two empirical parameters (Keller and Frisehknecht, 1966). For most sedimentary rocks, *a* is about 1 while *m* is about 2, for sucrossive rocks e.g. clean consolidated sandstones and carbonates. The resistivities of several types of ores are also shown. Metallic sulfides (such as pyrrhotite, galena and pyrite) have typically low resistivity values of less than 1 Ωm. Note that the resistivity value of a particular ore body can differ greatly from the resistivity of the individual crystals. Other factors, such as the nature of the ore body (massive or disseminated) have a significant effect. Note that graphitic slate has a low resistivity value, similar to the metallic sulphides, which can give rise to problems in mineral

surveys. Most oxides, such as haematite, do not have a significantly low resistivity value. One of exceptions is magnetite. The resistivity values of several industrial contaminants are also given in figure. Metals, such as iron, have extremely low resistivity values. Chemicals that are strong electrolytes, such as potassium chloride and sodium chloride, can greatly reduce the resistivity of ground water to less than 1Ωm even at fairly low concentrations. The effect of weak electrolytes, such as acetic acid, is comparatively smaller. Hydrocarbons, such as xylene ($6.998x10^{16}$ Ωm), typically have very high resistivity values. However, in practice the percentage of hydrocarbons in a rock or soil is usually quite small, and might not have a significant effect of the bulk resistivity. As an example, oil sands in Figure1 have the same range of resistivity values as alluvium.

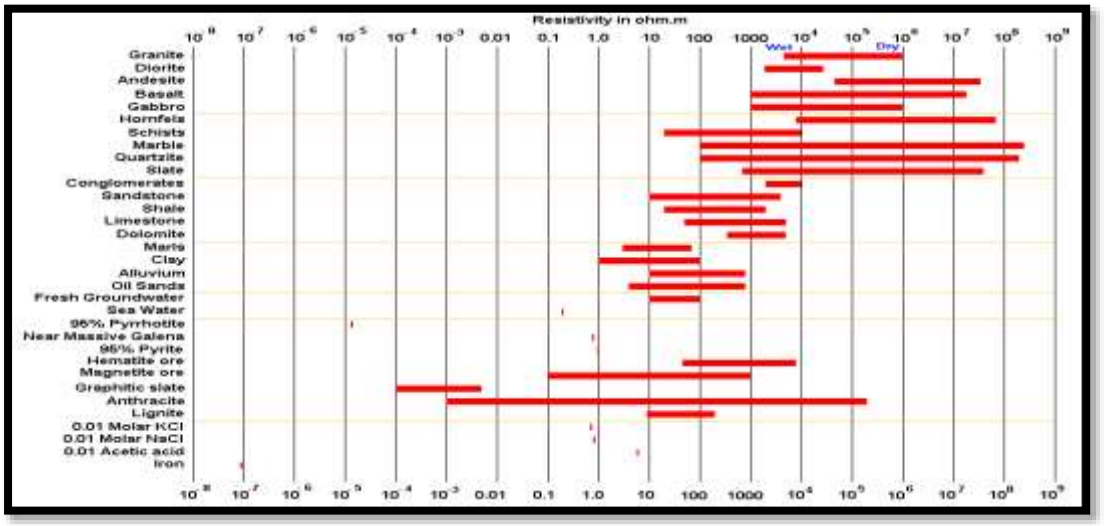


Fig. 1. Resistivity values for earth materials adopted for this work (Foster et al, 2000).

**Seismic Refraction Tomography**

The geophysical method used for this study is seismic refraction and the technique is refraction tomography. Tomography is an inversion program where measurements are made of energy that has propagated through a medium and the character of the energy received is then used to infer the properties of the medium through which it propagates. According to (Charles and William, 2005) tomography is an imaging technique which generates a cross-sectional picture (a tomogram) of an object by utilizing the object's response to the non destructive, probing energy of an external source. In this research work, seismic ray tomography, which is a form of travel time inversion used to determine lithologic velocity was used.

Seismic refraction tomography uses first arrival as input (Zhu and McMechan, 1989); (Stefani, 1995); (Zhu, 2002). The solution involves minimization of the difference between the observed travel times and those predicted by ray tracing through an initial model. The solution is iterative and contains five steps:

i. Picking of first arrivals.
ii. Ray tracing through an initial estimate of the velocity model.
iii. Segmenting ray paths into the portion contained in each cell of the velocity model.
iv. Computing the difference between the observed and predicted travelled time for each ray and
v. Iteratively back projecting the time differences to produce velocity model updates (Zhu, 2002).

**Seismic waves (Elastic waves)**

Seismic waves (Elastic waves) are classified into two principal waves, known as body and surface waves. In the Seismic body waves, when stress is applied to an elastic body the corresponding strain is propagated outward as an elastic wave. There are two types of waves that are propagated within the main mass of the Earth. The first type is variously known as a dilatational, longitudinal, irrotational, compressional or P wave, the latter name being due to the fact that this type is usually the first (primary) event on an earthquake recording. The second type is referred to as shear, transverse, rotational or S wave (since it is usually the second event observed on earthquake record).

i. In compressional waves the particles of the medium move in the direction of the wave travel. The compressional waves are the fastest of all seismic waves, when an earthquake or explosion occurs; this wave is the first to arrive at a recording station. As a result it is called a primary wave, or P wave (Charles and William, 2005). The compressional (or longitudinal) body wave passes through a medium as a series of dilatations and compressions. The equation of the velocity of the compressional wave is given by this relationship in equation (9) and (10).

$$V_p = \sqrt{\{k + \frac{\left(\frac{4\mu}{3}\right)}{\rho}\}} \qquad (9)$$

$$V_P = \sqrt{\frac{(1-\sigma)\epsilon}{(1+\sigma)(1-2\sigma)\rho}} \qquad (10)$$

where σ is the measure of stress, k is bulk modulus and ρ is the density of medium.

For shear or S-wave, the motion of particles of the wave is perpendicular (transverse) to the direction of the wave travel. The particles of a body vibrate in a direction of the wave in transverse waves. The equation of the velocity of the shear wave is given by the relationship in equation 11 and 12.

$$V_s = \sqrt{\frac{\mu}{\rho}} \qquad (11)$$

$$V_s = \sqrt{\frac{\epsilon}{2\rho(1+\sigma)}} \qquad (12)$$

The quantities λ and μ are known as Lame constants, k, is the bulk modulus, σ is a measure of the stress and ρ, is the density of the medium. Liquids and gases do not allow shear waves to propagate through them. Consequently μ = 0, and compressional wave velocity in a fluid is given by:

$$V_s = \sqrt{\frac{k}{\rho}} \qquad (13)$$

The only elastic property that determines the velocity of shear waves is the rigidity or shear modulus. In liquids and gases μ is equal to zero and shear waves cannot propagate in them (Charles and William, 2005).

Seismic Surface waves, just as the body waves, can be classified into two types: Rayleigh waves and Love waves, which are distinguished from each other by the type of particles motion in their wave fronts.

**Velocities of Earth Materials adopted for this Study**

Figure2 shows the P -wave velocity of the earth materials used in this work.

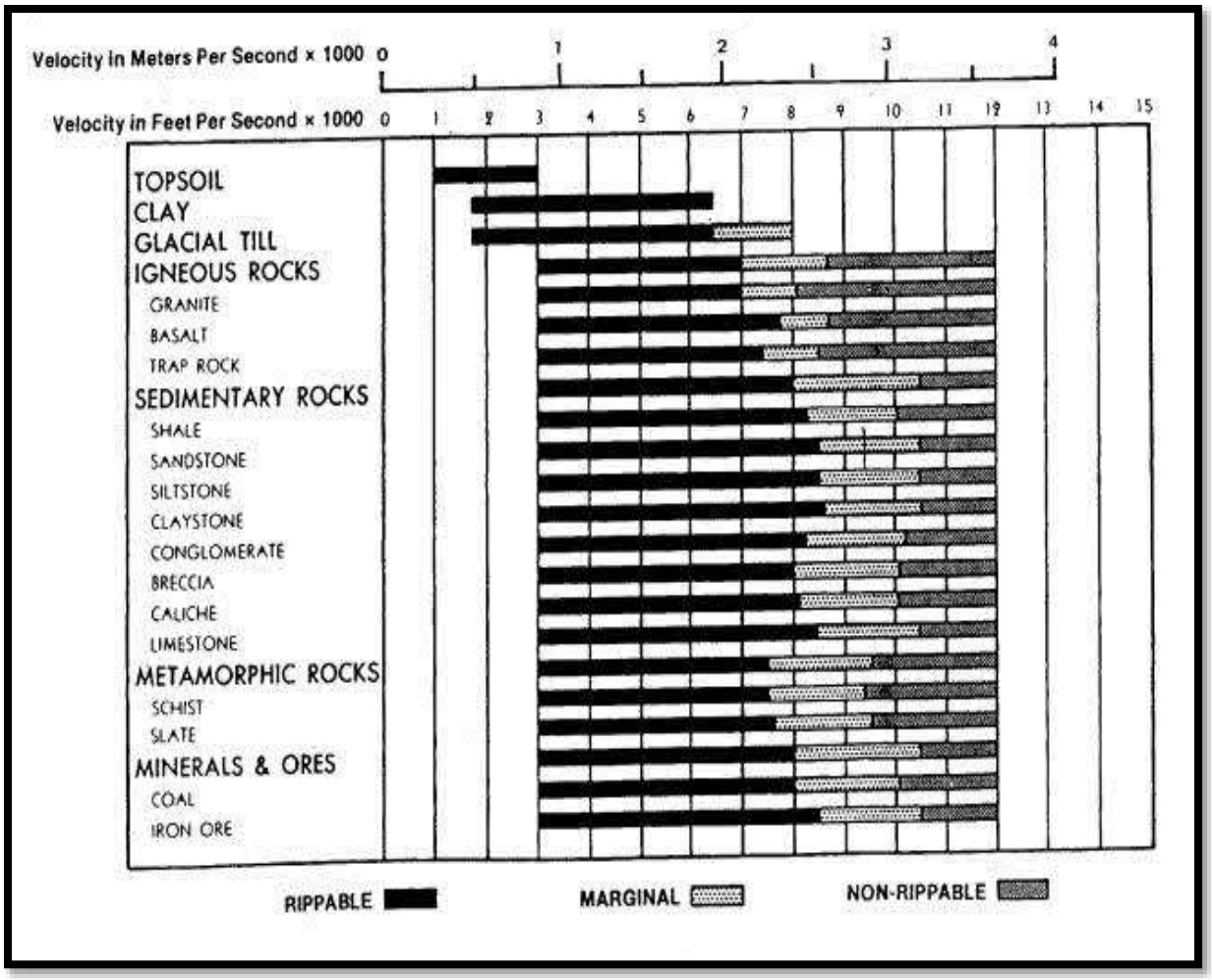


Fig. 2: p-wave velocity of earth materials (Kearey et al, 2002).

**Survey Area**

The Agban profile is located at latitude of $09^0$35'19.98"N and longitude of 08°22'25.38"E at Kaura area of Kaduna state. The area is fairly rugged (topographically) and located at the bottom western part of the Kagoro hill (Figure 3). Agban is underlain by gneisses and granite gneisses with several surface outcrops in form of domes and whaleback. The environs surrounding Agban is made up of the rocks of the Migmatite-Gneiss Complex, Older Granites, Younger Granites and Newer Basalts. Basement rocks that occur in the

study area could be classified into; Newer Basalts, Younger Granites, Older Granites, Undifferentiated Schists and Migmatites-Gneiss Complex.

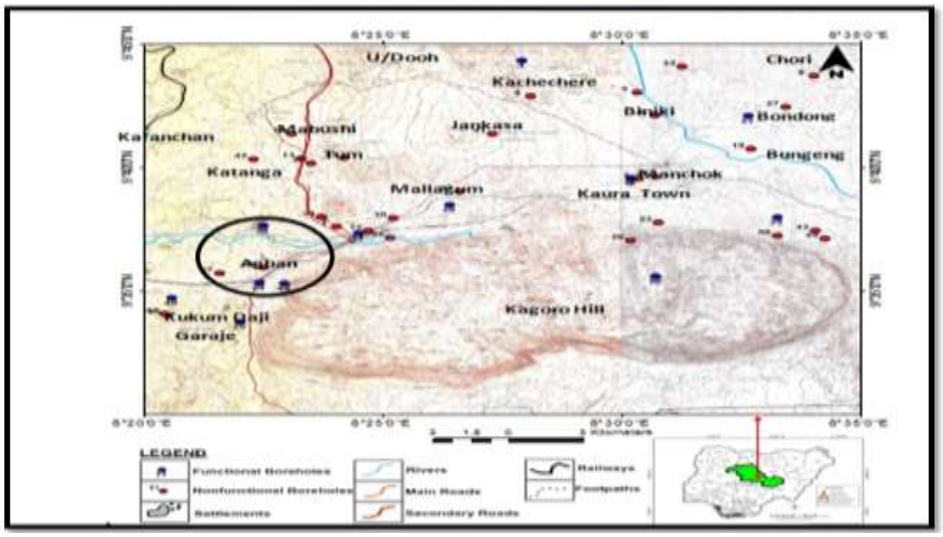


Fig. 3: Survey area showing Agban in circle (Afuwai et al, 2014).

## MATERIALS AND METHODS

### Materials

In this work, for the electrical resistivity survey, the instruments used for data acquisition are ABEM S.A.S. 300 Terrameter for measuring current and voltage, electrodes, cables and reels. GPS was used for situating and collecting the coordinates. The Terrameter consists of two units, the outer box containing both the Terrameter unit and the receiver, and the lower chamber consists of the rechargeable battery. These are assembled in rugged Aluminium boxes capable of withstanding rough transport and field conditions. Thus, the boxes give excellent protection to the electronic circuitry and other sensitive component parts of the instrument. The instrument is completely waterproof and the casing sealed against dust and dampness. It has a dial which is used to balance the resistivity of the ground set up due to the passage of current into the ground. For the Seismic refraction survey, a 24-channel Seistronix RAS-24 seismograph was used with a sledge hammer striking a rubber plate as an energy source and a shot-point at each geophone position.

### Data collection in electrical resistivity survey

Vertical Electrical Soundings (VES) using Schlumberger array were carried out at different points along an E-W profile. The profile was deliberately taken across a borehole. The largest Current electrode spacing AB used was 200m, that is, $\frac{AB}{2}$=100m. The principal instrument used for this survey is the ABEM Signal Averaging System, **(**SAS 300) Terrameter. The resistance readings at every VES point were automatically displayed on the digital readout screen and then written down on paper. The geometric factor, K, was first calculated for all the electrode spacings using the formula; $K = \pi\ (L^2/2b - b/2)$, for Schlumberger array with MN=2b and $\frac{AB}{2}$=L. The values obtained, were then multiplied with the resistance values to obtain the apparent resistivity, $\rho_a$, values. Then the apparent resistivity, $\rho_a$, values were plotted against the electrode spacings ($\frac{AB}{2}$) on a log-log scale to obtain the VES sounding curves using an appropriate computer software *IPI2win+IP*. Three resistivity sounding curve types were obtained from the studied area and these are the H ($\rho1>\rho2<\rho3$), A ($\rho1< \rho2<\rho3$) and KH ($\rho1>\rho2< \rho3>\rho4$) type curves. The VES profiles were correlated and merged with respect to the direction of the profile line and the closeness of the individual VES stations. On the pseudo sections, the top horizontal scale represents the names of the sounding points, while the bottom horizontal ruler represents the coordinates of the sounding points. Vertical lines mark the sounding point given as *AO (m)* being equivalent to half the current electrode spacing, *AB/2*. The interpretation made for each tomogram is placed by its side. A log of the borehole along each profile and the geology of Kagoro Area aided the interpretation.

### Data Collection and Processing in Seismic Refraction Tomography

The field procedure involves laying out the spread with the shot and the receivers in a straight line. The receivers are placed at an interval of 5m, which resulted in a total spread length of 120m for twenty four vertical geophones. Shots were fired at the beginning and at the end of the profile, and at each receiver point. The seismic signals generated are properly recorded with the digital seismograph. In this work a 24-channel Seistronix RAS-24 seismograph was used with a sledge hammer striking a rubber plate as an energy source and a shot-point at each geophone position. Data were stacked at least four times for each shot. Throughout the survey the geophones were placed at an interval of 5m along profile. The profile was deliberately taken across the borehole location. The software ReflexW developed by Sandmeier, (2003), was used to perform the data processing and to interpret the seismic refraction tomography data. The data collected from the field was subjected to different stages of processing to enhance the signal-to-noise ratio. The data was first filtered

by applying a band pass filter (with an upper and lower frequency of 150Hz and 50Hz respectively) to improve the quality of the real signal. First-arrival travel times were picked manually and ray paths were calculated by the ray tracing method based on Huygen's principle (Parasnis, (1997).

**RESULTS AND DISCUSSIONS**

The data analysis was performed using IPI2Win+IP method for the automatic interpretation of schlumberger sounding curves. This method was used to obtain the model for the apparent resistivity of each sounding. The resulting true resistivity layer model from the application is shown in figure 4. The true resistivity models at every sounding point along each profile were used to produce the geoelectric Pseudo section for that profile.

Based on the IPI2Win's method, the field curves were found to be averagely four (4) layers. Below are some examples of resistivity models obtained in the survey.

Osazuwa et al, 2008 Wrote on the topic: Improved depth of penetration of geoelectric imaging in a confined area (Lokoja new general hospital in Kogi State) using refraction tomography, showed that seismic refraction tomography probes deeper than geoelectric tomography at the same spread length. This is because in seismic refraction method the receiver array arranged along the spread is several times the depth of interest. It has also been established that in seismic refraction the depth of probe is $^1/_5\,th$ of the spread length, while in electrical resistivity survey, using vertical electrical sounding the depth of probe is $^1/_3\,th$ of the spread length. Also, because the resistivity method is sensitive to tiny variations in the conductivity of the near surface, more subsurface layers are detected than in the seismic refraction survey.

The Borehole at Agban is functional. It is located at latitude of $09^0$35'19.98"N and longitude of 08°22'25.38"E. Ten (10) VES Points were sounded at different points along a profile of 200m in the W-E direction. The borehole was drilled to a depth of 40m with an initial yield of 17litre/min. Figure4 shows the Resistivity tomography section for Agban I profile. The interpretation of resistivity section shows that the profile constitutes of five (5) layers namely; the Overburden comprising wet sandy clay, the weathered basement which constitutes of water and sand with little traces of sandy clay at VESagb8, the partially weathered basement with resistivity range of 133-178Ωm composed of fine grain sand, the fractured basement comprises of coarse grain sand with resistivity range of 237-316Ωm, the fifth layer is the fresh basement rock (Figure 5). This interpretation is in agreement with the borehole log of the Borehole located in between VESagb4 and VESabg5. This Borehole was drilled to a sufficient depth through an aquifer with significant thickness and favourable initial yield, and the degree of weathering and fracturing of the subsurface structures across this profile is substantial to sustain the borehole.

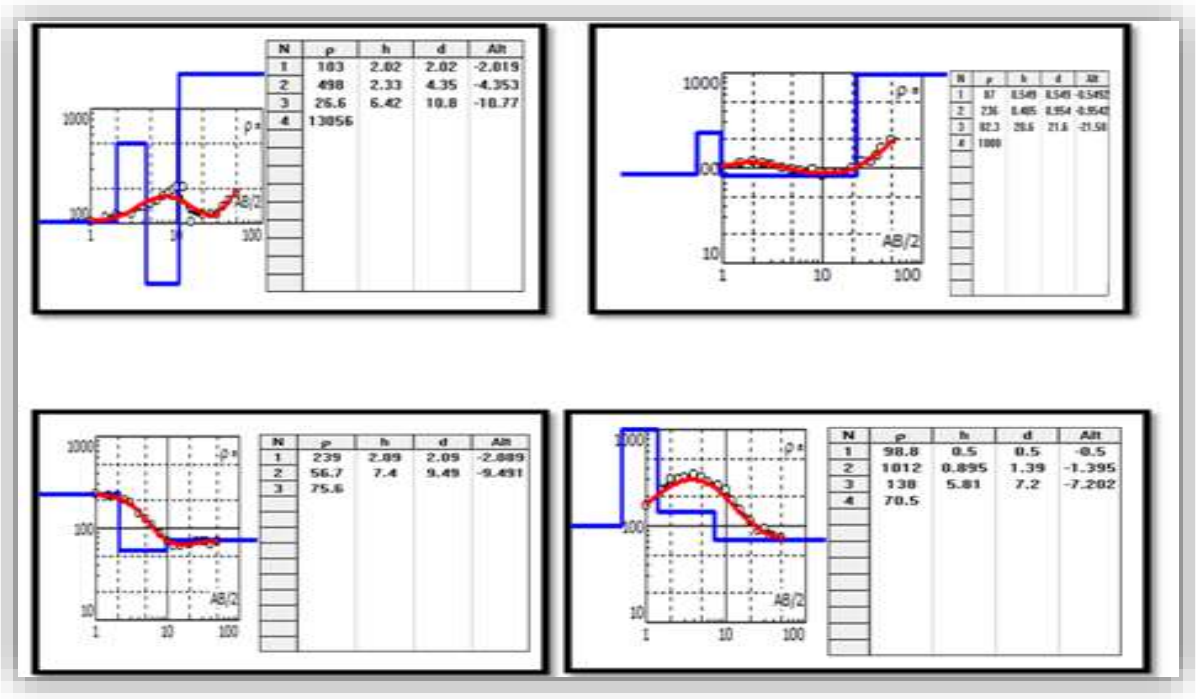


Fig. 4: VES Curves where Layer resistivities, depths and thickness were obtained

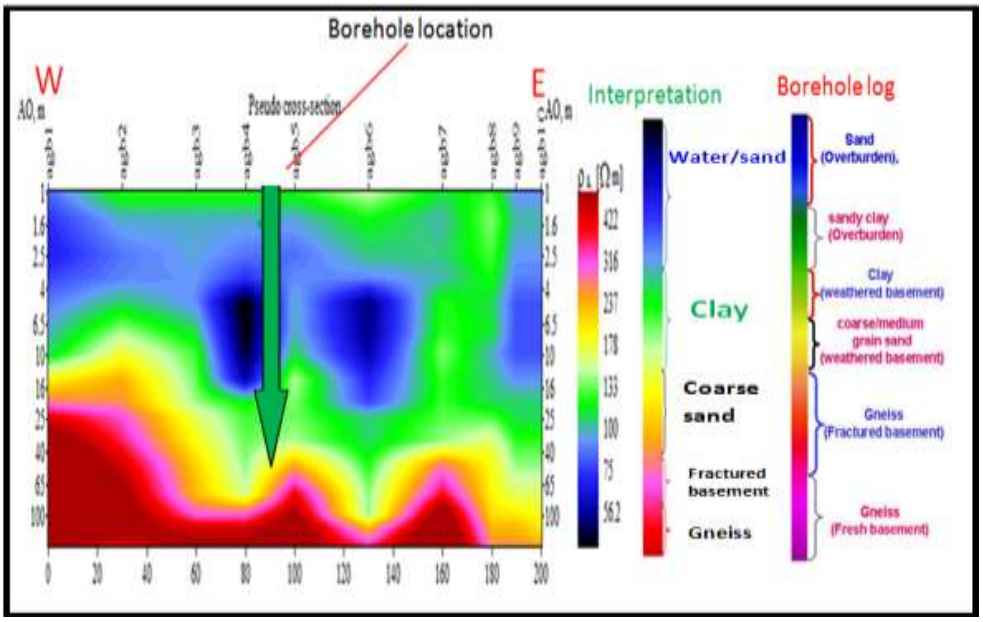


Fig. 5: Resistivity tomography section for Agban I Profile

The Seismic Refraction tomography results (Figur6) suggest that the Agban profile at shallow depths is predominantly characterized by four (4) layers having relatively low p-wave velocities (327m/s) at its uppermost layers and relatively high velocities of over 2420m/s at depths. According to Adedibu and Abimbola (2019), the range of the velocity measured (327 - 2500 m/s) encompasses the p-wave velocities of sand (320 - 800 m/s), sandy clay (850 - 1250m/s) and clay (900 – 25000 m/s) which occur at shallow depths (24m) while at depths, occur coarse grain sand (weathered basement) of p-wave velocities (1500-30000m/s) and porphyritic granite (fresh basement) of range 2000–45000 m/s. Aquiferous zones (1200 m/s – 1500 m/s) occur between the depths of 12m and 25m. The Borehole at Agban I is functional. It is located at latitude of $09^{0}$35'19.98"N and longitude of 08°22'25.38"E. The borehole was drilled to a depth of 40m with an initial yield of 17litre/min. This Borehole was drilled to a sufficient depth through an aquifer with significant thickness and favourable initial yield, and the degree of weathering and fracturing of the subsurface structures across this profile is substantial to sustain the borehole.

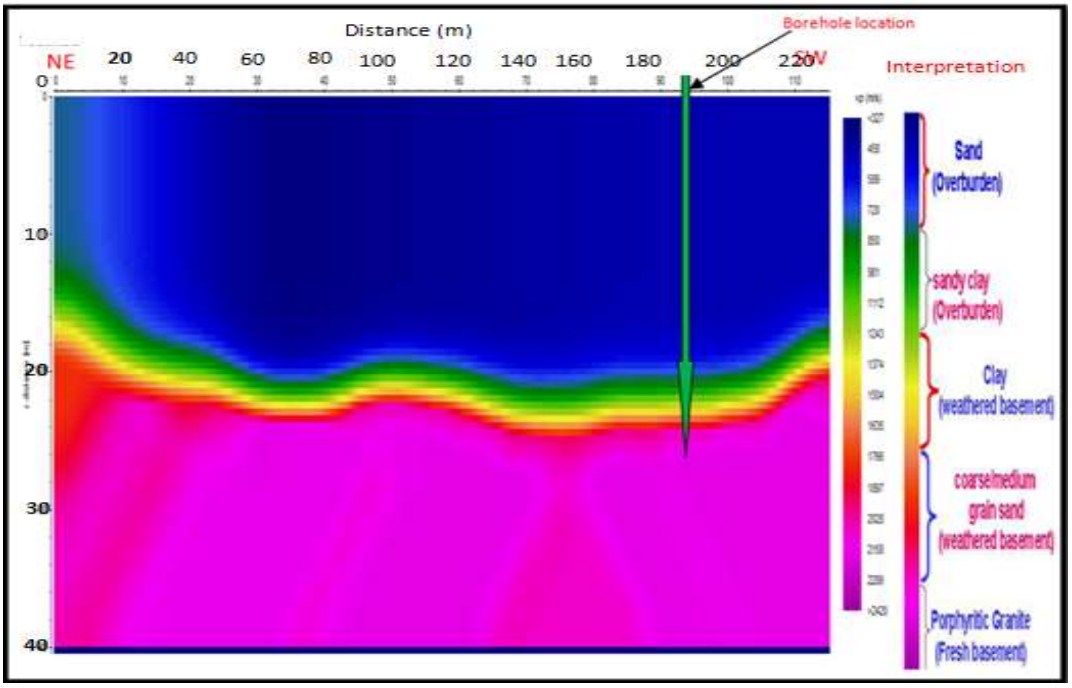


Fig. 6: Seismic model for Agban Profile

## CONCLUSION

The following was arrived at after the survey: In the Geoelectric section along a spread length of 200m, a depth of 65m was investigated. In the Seismic refraction tomography along a spread length of 200m, a depth of 40m was investigated. In the Geoelectric section, five (5) subsurface layers were detected; the topsoil comprising wet sandy clay, the weathered basement which constitutes of water and sand with little traces of sandy clay at VESagb8, the partially weathered basement with resistivity range of 133-178Ωm composed of fine grain sand, the fractured basement comprises of coarse grain sand with resistivity range of 237-316Ωm, the fifth layer is the fresh basement rock. The Seismic refraction tomogram shows that the area is predominantly characterized by four (4) layers having relatively low p-wave velocities (327m/s) at its uppermost layers and relatively high velocities of over 2420m/s at depths. The range of the velocity measured (327 - 2500 m/s) encompasses the p-wave velocities of sand (320 - 800 m/s), sandy clay (850 - 1250m/s) and clay (900 – 25000 m/s) which occur at shallow depths (24m) while at depths, occur coarse grain sand (weathered basement) of p-wave velocities (1500-30000m/s) and porphyritic granite (fresh basement) of range 2000–45000 m/s. Aquiferous zones (1200 m/s – 1500 m/s) occur between the depths of 12m and 25m.

## REFERENCES

Adedibu SA and Abimbola CO. (2019). Insight into seismic refractionand electrical resistivity tomography techniques in subsurface investigations. The Mining Geology Petroleum Engineering Bulletin, Vol 550(1) Pp 93-111.

Afuwai G.C. and Lawal K.M. (2013). Interpretation of Vertical Electrical Sounding Points around two boreholes at Samaru College of Agriculture ABU, Zaria-Nigeria. Scholars Research Library, Archives of Physics Research. 4(5). 49-54.

Afuwai, G.C., Lawal, K.M., Sule, P and Ikpokonte, A.E. (2014). Geophysical Investigation of the Causes of Borehole Failure in the Crystaline Basement Complex: A Case Study of Kaura Area of Kaduna State, Nigeria. *Journal of Environment and Earth Science*, 4(23). 131-141.

Charles F. Narwold and William P. Owen (2005). Seismic refraction Analysis of landslides. *Geophysics and geology*, 31(4), pp 8-12.

Foster, S. S. D., Chilton P. J., Moench M., Cardy F. and Schiffler M. (2000). Groundwater in rural development, World Bank Technical Paper No 463, The World Bank, Washington D C.

Grant FS, West GF (1965). Interpretation Theory in Applied Geophysics. McGraw-Hill, New York.

Kearey P., Hill I. and Brooks M. (2002). An Introduction to Geophysical Exploration (Ed). Tj International Ltd., Padstow, Cornwall, United Kingdom, 21-122.

Keller, G. V. and Frisehknecht, F. C., (1966). Electrical methods in geophysical Prospecting pergamon Press.

Lowrie, W. (1997). Fundamentals of geophysics. *Cambridge University press*. Location Map Zaria, Sheet102. Osazuwa, I.B., Chiemeke, C.C., Abdullahi, N. K., Akaolisa, C.C. (2008); Improved Depth of Penetration of Geoelectric Imaging in a Confined Area Using Refraction Tomography. *Journal of Environmental Hydrology* Volume 16. On the World Wide Web at http://www.hydroweb.com

Osazuwa, I.B., Chiemeke, C.C., Abdullahi, N. K., Akaolisa, C.C. (2008); Improved Depth of Penetration of Geoelectric Imaging in a Confined Area Using Refraction Tomography. *Journal of Environmental Hydrology* Volume 16. On the World Wide Web at http://www.hydroweb.com

Parasnis, D.S., (1997). Principles of Applied Geophysics, fifth ed., Chapman and Hall, London.

Sandmeier K.J. Windows™ 9x/NT/2000/XP-program for the processing of seismic, acoustic or electromagnetic reflection, refraction and transmission data, Manual for REFLEXW 2003. 3:1-177. ( available at www.sandmeier-geo.de).

Stefani, J.P. (1995). Turning ray tomography. *Geophysics*, 60, 192-193.

Zhu, X., and McMechan, G. A. (1989). Estimation of two dimensional seismic compressional wave velocity distribution by iterative tomography imaging. *Journal of imaging system technology*. 1, 13-17.

Zhu, X. A., (2002). Velocity imaging through complex near-surface structures. ECGE64th conference and exhibition; PGS Geophysical research division, 10550 Richmond Avenue, Houston, TX77042, U.S.A.,54-61.